Astron. Astrophys. 312, 525–538 (1996)

ASTRONOMY AND ASTROPHYSICS

NLTE models for synthetic spectra of type Ia supernovae

The influence of line blocking

A.W.A. Pauldrach[1], M. Duschinger[2,1], P.A. Mazzali[3], J. Puls[1], M. Lennon[1], and D.L. Miller[4]

[1] Institut für Astronomie und Astrophysik, Scheinerstr. 1, D-81679 München, Germany
[2] Max-Planck-Institut für Astrophysik, Karl-Schwarzschild-Str. 1, D-85748 Garching b. München, Germany
[3] Osservatorio Astronomico, Via G.B. Tiepolo, 11, I-34131 Trieste, Italy
[4] Department of Physics and Astronomy, University of Pittsburgh, 3941 O' Hara Street, Pittsburgh, PA 15260, USA

Received 12 September 1995 / Accepted 16 December 1995

Abstract. A method to compute a NLTE model of the atmosphere of a type Ia supernova (SN Ia) near maximum light is presented. The determination of the level populations is carried out using detailed atomic models, and including all important contributions to the rate equations: Thomson scattering, bound-free (from ground and excited levels) and free-free opacities, line absorption and emission processes. Dielectronic recombination is included. The spherical radiation transfer is solved at up to 400 frequency points and 41 depth points. Finally, a synthetic spectrum is computed using a formal integral solution of the transfer equation based on a spatial microgrid.

It is found that the SN atmosphere is electron scattering-dominated, and that the high velocity of the apparent photosphere ($\sim$ 8000 km/s) is due to the pseudo-continuum opacity created by the thick line forest which blocks the flux in the UV and optical part of the spectrum. Increasingly more sophisticated treatments of the process of flux blocking in the UV (line blocking) are discussed. The necessity of treating the far-UV flux correctly is demonstrated. Line blocking in the region 800–1300 Å reduces the photoionization from the excited levels of several important ions (e.g. Fe II, Co II, Si II, Ca II), thus decreasing the overall degree of ionization. This effect is clearly seen in the synthetic emergent spectra.

Synthetic spectra obtained with the various methods adopted for line blocking are shown, and compared to one another. When line blocking is properly treated, the synthetic spectrum reproduces well the spectrum of the 'normal' SN Ia 1992A from the UV to the near-IR.

Key words: radiative transfer – stars: atmospheres – supernovae: general

Send offprint requests to: M. Duschinger

1. Introduction

Supernovae (SNe) are interesting objects in astrophysics because they represent the most drastic end-point of stellar evolution. They feed back the heavy elements synthesized in stellar interiors from the primordial H and He into the interstellar medium and thus give rise to the process of chemical evolution of galaxies. Because of their large energy release, SNe are very bright events, and can be observed at cosmological distances.

Type Ia SNe (SNe Ia) appear to be the brightest SNe, and to form the most homogeneous group both photometrically and spectroscopically. Their light curve shows a rapid rise to maximum (15–20 days) followed initially by a fast drop and subsequently by an exponential tail, which is governed by the deposition of the γ-rays produced by the decay of ^{56}Co. Their spectra show no H lines, but rather a strong Si II line near 6100 Å, and lines of Fe II, Co II and Ca II. SNe Ia were soon identified as potentially strong candidates for standard candles in cosmic distance studies. It is therefore extremely important to understand the process giving rise to these objects and the properties of the progenitor stars.

In the standard picture, SNe Ia are thought to be the result of the explosion of CO white dwarfs (WDs) in binary systems, the explosion occurring when the WD approaches the Chandrasekhar mass limit of $1.4M_{\odot}$ by accretion from an evolved companion (Nomoto et al. 1984). The burning front is supposed to proceed subsonically (deflagration wave), burning the core matter into nuclear statistical equilibrium and producing about $0.7M_{\odot}$ of ^{56}Ni. Outside the ^{56}Ni core Intermediate Mass Elements (Si, Ca, S, Mg) are synthesized, while a thin outer CO layer is supposed to remain unburned.

In recent years, a number of SNe Ia have been discovered which do not fit the standard Ia description, especially from the spectral point of view. In particular, SN 1991T showed before maximum lines of Fe III rather than the usual Fe II and Si II ones, and was probably an overluminous object (Mazzali et al. 1995), while SNe 1991bg and 1986G were redder than normal

and displayed spectral peculiarities which lead to the conclusion that they are subluminous (Filippenko et al. 1992, Mazzali et al. 1996, in prep.). Since these objects are identified as non-standard mostly from their spectra, it becomes very important to develop a model for the formation of SN spectra that describes as accurately as possible all physical processes present in the objects. This is at the basis of the present work.

For about one month after explosion the SN is in the 'photospheric' epoch. This is the epoch when the density in the ejecta is still high enough that a pseudo-photosphere appears to form, while the expanding ejecta above that photosphere leave their mark in the form of broad P-Cygni profiles, much as in the winds of hot stars. The main difference here is that the expansion velocities are very large (> 10000 km/s), while the photospheric temperature is not so high ($T \sim 10000$ K).

The spectra at this epoch contain useful information on the energetics of the explosion (luminosity, velocity) and on the nucleosynthesis in the intermediate and outer part of the WD, i.e. in the shells that lie above the momentary pseudo-photosphere. In the past, several groups have computed synthetic spectra for SNe Ia in the photospheric epoch, all of them using some simplifying assumptions: in particular, Branch et al. (1985) adopted parameterized level populations to model SN Ia spectra, while Jeffery et al. (1992) and Kirshner et al. (1993) used an LTE code, none of which incorporated continuum transfer. Harkness (1991) also assumed LTE conditions in his spectrum synthesis calculations, but additionally included continuum transfer. Nugent et al. (1995) calculated synthetic spectra for SNe Ia in NLTE, but only for Ca II, Mg II and Na I. Höflich (1995) also performed a NLTE calculation, but considered only C II, O II, Ne I, Na I, Mg II, Si II, S II, Ca II and Fe II. Finally, Mazzali & Lucy (1993) used a quasi-NLTE model, where the radiation transport was performed by means of a Monte Carlo (MC) method.

In this work, we describe the computation of synthetic spectra for SNe Ia using a NLTE code, which includes, in addition to the inherent radiative transfer required for the computations of the rate equations, a formal integral solution of the transfer equation based on a spatial microgrid which is used to calculate the synthetic spectrum. The code was developed to compute consistent models for expanding envelopes of hot stars (Pauldrach 1987, hereafter Paper III; Pauldrach et al. 1994, hereafter Paper XII). In the following sections we discuss the basic concept (Sect. 2) and how the code had to be adapted so that it could deal with a SN atmosphere, extending the method already outlined in Branch et al. (1991, hereafter ELBA) (Sect. 3). In Sect. 4 we discuss the SN Ia against whose spectrum we compare our models, SN 1992A, and its importance as a test of line blocking calculations, and present the treatment of line blocking in the UV. We then discuss (Sect. 5) the various methods used to compute line blocking, and show the fits to the spectrum of SN 1992A from the UV to the near-IR.

Table 1. Summary of atomic data

Ion	Number of packed levels	Number of levels	Total NLTE lines	Total Lines
C II	36	88	284	11005
O I	48	184	534	18399
O II	50	142	595	39206
O III	50	118	565	26493
Mg II	26	52	104	3778
Si II	40	92	293	4560
Si III	50	98	480	4046
S II	50	138	592	27767
Ca II	28	56	133	3067
Ti II	50	136	509	56684
Ti III	50	100	482	8786
Cr II	50	160	321	221932
Cr III	50	130	447	165517
Cr IV	50	134	486	63757
Mn II	50	156	305	227761
Mn III	50	158	364	223333
Fe II	50	176	405	227550
Fe III	50	150	246	264366
Co II	50	140	482	189859
Co III	50	164	469	236656
Ni II	50	152	419	129792
Ni III	40	112	281	133249

2. Basic concept

In order to compute synthetic SN Ia spectra we have adapted our stellar wind code. This code is based on the concept of a homogeneous, stationary, spherically symmetric outflow, which describes the time average mean of most features in the UV spectrum of hot stars, and was described in several papers (Paper III, Paper XII). The analogy between a hot star wind and a SN in the photospheric epoch is that in both cases the spectrum is the result of the superposition on the photospheric continuum of the spectral lines formed within an expanding atmosphere, but there are important differences, which we list below.

First, in a SN the photosphere is actually not a physical boundary, and is not constant in position (in both radius and velocity coordinates) with time. Nevertheless, at any given time snapshot the analogy can be made.

Secondly, in SN Ia ejecta the dominating elements are not H and He, with their relatively simple atomic structure, but much heavier ones, like O, Si, Fe, Co. In view also of the low temperature in a SN atmosphere, it becomes very important then to use accurate atomic models in the NLTE code even for singly and doubly ionized species.

Thirdly, due to the large velocity gradients in a SN envelope ($v \propto r$), the UV part of a SN Ia spectrum, which is otherwise almost free from continuous absorption (the redmost important ground state ionization edge for the typical composition of the SN Ia ejecta being Ca II at 1044Å), is effectively blocked by the superposition within the expanding envelope of the thousands

of strong metal absorption lines. Since the SN is in a state of homologous expansion, each point within the envelope sees all the other points receding from it. Thus, a photon emitted at the photosphere will be redshifted in the co-moving frame as it moves outwards in the envelope, and it will be brought into resonance with redder and redder lines. The number of such lines can be very large, since the envelope matter can reach velocities of the order of 20,000 km/s. In the UV, where the metal lines crowd very densely, this line overlap becomes in practice a source of continuum opacity. A UV photon can only escape if it scatters its way out, becoming a redder photon, until it finds a low-opacity window in the spectrum.

An appropriate treatment of such an effect is of great importance for the computation of synthetic SN spectra, because the blocking occurs just in the wavelength region where the radiation emitted from the photosphere reaches its peak intensity (photospheric temperatures are typically of the order of 10000 K near maximum light). The high velocities complicate the problem compared to O stars, since the number of spectral lines which are brought into resonance at different depths in the envelope is much larger. On the other hand, the large velocity gradient and the linear dependence of velocity on radius simplifies the problem, since it does not favour a large line overlap and makes the calculation of resonant surfaces much easier than in the case of an accelerating flow, typical of stellar winds.

The effect of line blocking is to reduce the intensity of the radiation field in the UV. An important difference is that in SNe Ia the spectral region where the important line blocking process occurs falls in the near UV (1000–3500 Å), since the photospheric temperature of a SN Ia near maximum light is cooler than in hot stars, and so the ionization regime is lower and line blocking is due mostly to species such as Fe II, Co II, Si II. This spectral region is accessible to orbiting telescopes (IUE, HST). In O stars, on the other hand, the strong blocking occurs at $\lambda < 911$ Å, and such regions cannot be observed. The observation of the flux in the line blocking region allows line blocking calculations to be directly compared with observations, instead of having to rely blindly on models.

Line blocking has an effect not only on the emergent spectra but also, indirectly, on the level populations, since the rate of ionization from excited levels occuring at wavelengths corresponding to the line-blocked region is reduced. Thus, an iterative scheme including line blocking is required to compute the level populations and the radiation field consistently.

3. Method

The method used for our calculations was briefly described in ELBA, and, for the O star case, in Paper XII. Here we discuss the major improvements implemented since that work.

First we select velocity and density profiles from a SN explosion model (in our case the 'standard' deflagration model W7(Nomoto et al. 1984)), then we solve iteratively the rate equations in NLTE and the equation of radiative transfer in the SN atmosphere using an Accelerated Lambda Iteration (ALI) (Pauldrach & Herrero 1988).

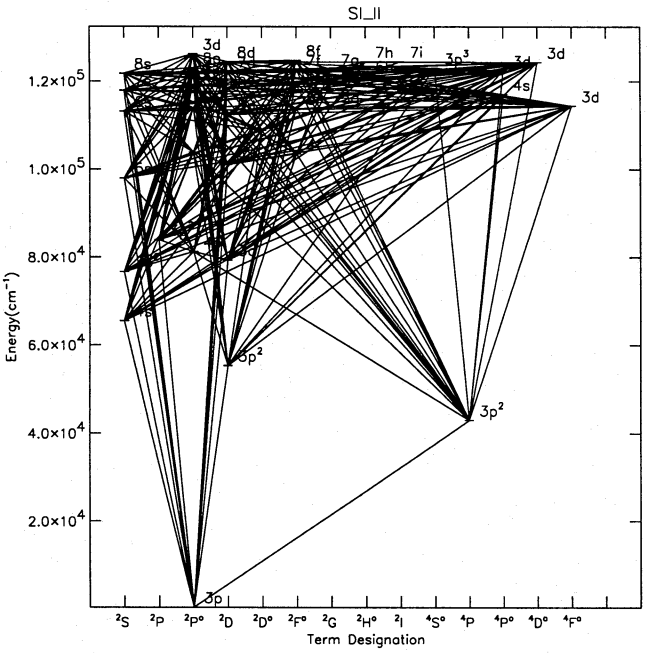

Fig. 1. Grotrian diagram of Si II as used in the calculations.

We now describe the main characteristics of the SN atmosphere model needed to compute synthetic spectra that take the SN physical conditions into proper account.

In a SN, the position of the photosphere changes with time as the ejecta expand. Roughly speaking, a specific point (e.g. $\tau_{\rm Ross} = 1$) falls at a constant density, so that it moves deeper into the ejecta (i.e. to lower velocities) with time. We adopt as an inner boundary the diffusion approximation, and we compute our model down to $\tau_{\rm Ross} \sim 10$, which occurs almost at the centre of the ejecta. In SN ejecta, in fact, the density does not become very large at very low velocities since $\rho(r)$ is a power law, which is flatter than the exponential law that applies to stars. All the important opacities and emissivities are included in the calculation: Thomson scattering, bound-free (from ground and excited levels) and free-free opacities and line absorption and emission processes.

In the SN atmosphere the opacity due to lines from excited levels is very important: the relatively flat density profile in a SN favours the population of the excited levels, and, in general, leads to a higher degree of ionization than is found in stars of similar effective temperature, which have different effective gravities and abundances. Photoionization from excited levels is favoured over photoionization from the ground state because the excited states absorb radiation from the optically thin part of the spectrum. Consequently, and in contrast to photoionizations from the ground state, the radiation temperature is much higher than the local temperature, and photoionization from excited levels proceeds efficiently. This is further enhanced since, with the SN Ia atmosphere composition, there is a high abundance of ions with high lying excited states from which photoionization at optical wavelengths can occur. Then again it is important to include very accurate atomic models. Our NLTE calculations

were based on our revised set of atomic models, computed using the SUPERSTRUCTURE code (Eissner et al. 1974) as described in Paper XII. We included the highly detailed models (with accuracy $\pm 10\%$) described in Paper XII for the following ions: O I–III; C I–IV; Si II–IV; S I–IV; Mg II and IV; Ca I–IV; Fe III and IV; Co III and IV; Ni III and IV. Since we found that the models by Kurucz (1992) are very similar to our calculations for Ni II and III, and are accurate to $\pm 20\%$, we used his models for Fe II; Co II; Ni II; Ti II and III; Cr II–IV. In total, our line list includes 5000 levels and more than 2,000,000 lines. In Table 1 we recap our data, and in Fig. 1 we show a representative Grotrian diagram for Si II that results from our calculations.

We use a static spherical grey temperature structure. In the outer layers we fix the temperature at a constant value of about 6000 K, since otherwise it would decrease to arbitrarily low values due to the nature of the spherical grey atmosphere. This method describes the atmosphere of SNe Ia in sufficient detail, since the conditions in the atmosphere depend mostly on the radiation field.

The occupation numbers are determined by the rate equations containing collisional (C_{ij}) and radiative (R_{ij}) transition rates. Apart from the lowest lying levels, where correct values are used, the photoionization cross sections are approximated as described in Papers III and XII. On the other hand, correct dielectronic recombination rates are included.

Correct radiation transfer is necessary, since the radiation field has the strongest effect on ionization and excitation, and thus on the occupation numbers and on the line opacities. The spherical transfer equation is solved, yielding the continuum radiation field at up to 400 frequency points for 41 depth points, including the deepest layers where the diffusion approximation is applicable.

Our procedure is as follows:

a) Continuum. A first iteration cycle is performed using the continuum opacities of the two most abundant elements, i.e. silicon and oxygen. Then the entire mixed SN Ia composition (9 elements: Si, O, C, S, Mg, Ca, Fe, Co, Ni, as given in ELBA and derived from W7, plus other less abundant elements) is used in a second iteration cycle until a converged radiation field $J_\nu(r)$ based on continuous opacity is obtained. Note here that free-free absorption is never very important in the case of a SN. Line opacity, which should be included at this stage, was kept separate and dealt with as follows:

b) Lines. For the calculation of the radiative rates the 'Sobolev with continuum' approximation (Puls & Hummer 1988) is used throughout the envelope. This is a sound approximation in a SN envelope, since the differential velocities attained there are very large, much larger than in hot star winds (Duschinger et al. 1995, Sellmaier & Pauldrach 1996, in prep.). Note that during the final iterations a continuum radiation field modified by line blocking (see below) is used in the Sobolev approach.

c) Line blocking. After including the lines in the rate equations using an ALI, we compute the effect of line blocking.

The effect of the continuum opacity in the far-UV and of the pseudo-continuum resulting from line blocking in the near-UV is to reduce the radiation field in those spectral regions, and thus to decrease all upward radiative rates (b–f and b–b) occurring at the corresponding frequencies. The intensity of the radiation at a given frequency at any depth in the envelope depends on the radiation input from the photosphere, as defined by the continuum opacity, and on the extent of line blocking at all depths in the atmosphere.

Due to the large velocity gradient in the envelope, only relatively few lines ($\sim 10^5$) are sufficient to give an accurate description of the effective line opacity and emissivity. Such a line reduction is performed by considering all the lines effective over a certain velocity interval. This procedure is important because the number of overlapping lines is otherwise very large, and is used in the consistent treatment of line blocking discussed in Sect. 5.3.

Since the correct treatment of line blocking requires lengthy calculations and may give convergence problems, and since it is not certain that line blocking is the only mechanism responsible for the observed depression in the UV flux, we initially simulated blocking with different methods, which can also be used to set constraints on the radiation field and to see whether the observed spectrum can be reproduced.

In one method, we looked at the emergent fluxes observed in the spectrum of the prototypical SN Ia SN 1992A and derived mean intensities J_ν consistent with these values (cf. Sect. 5.2.1). Since the observed energy distribution does not cover the entire wavelength range important for line blocking, we alternatively calculated J_ν values consistent with a synthetic spectrum computed with the MC code described by Mazzali & Lucy (1993) in order to reproduce the spectra of another 'standard' SN Ia, SN 1990N (Mazzali et al. 1993) (cf. Sect. 5.2.2). Finally, a calculation with an exact treatment of line blocking was performed (cf. Sect. 5.3). In each case, the resulting values J_ν have been used afterwards in the determination of the radiative rates R_{ij}.

d) Emergent spectrum. As a final step, a formal integral is performed to compute the emergent spectrum. The procedure adopted was described in Paper XII.

For the time being we are ignoring the ionizing effect of the fast electrons produced by the γ-rays from the decay of ^{56}Ni and ^{56}Co. Although in the SN explosion model we have adopted (W7) ^{56}Ni is expected to be synthesized only in the deepest layers, which lie well below the photosphere at the time of maximum, the probability that the γ-rays escape to the envelope before thermalizing is not negligible. Our present aim was, however, to describe the conditions in the SN atmosphere globally, to understand the results of a NLTE treatment of the rate equations and to assess whether our treatment gives us control over the most important physical processes. If this were the case, then we could analyze special effects such as the abundances and their stratification.

4. Models for SN1992A

In the present paper, where we discuss the main features of our model, we have tried to reproduce the observed spectrum

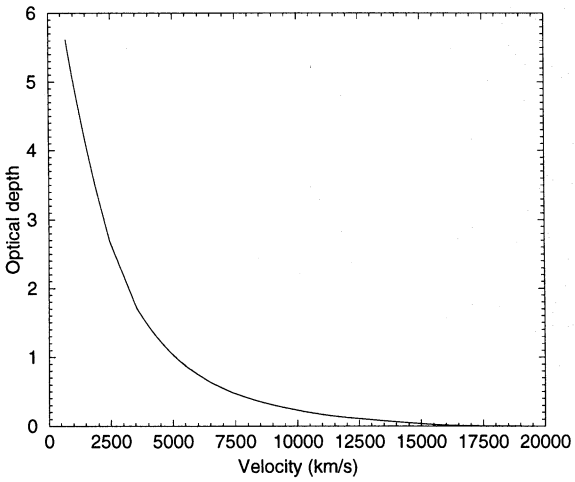

Fig. 2. The Rosseland optical depth ($\tau_{\rm Ross}$) with continuum opacity only (solid line) and the optical depth for Thomson scattering (dashed line) vs. velocity in the ejecta for the pure continuum model. The two curves are indistinguishable.

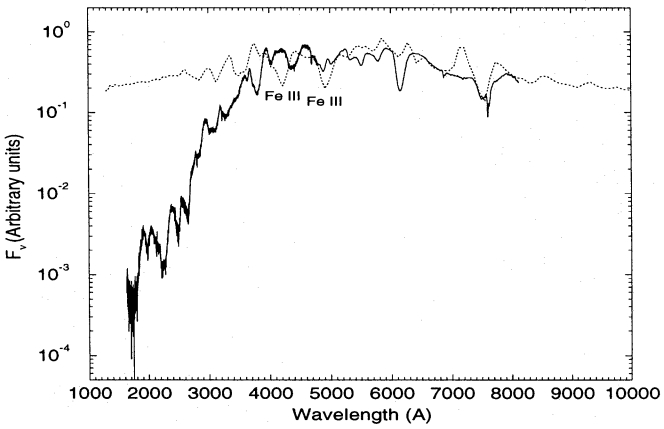

Fig. 3. The synthetic NLTE spectrum for the model without line blocking (dotted line) compared to the spectrum of SN 1992A (solid line).

of SN 1992A near maximum from the UV to the near IR. We have adopted this object as our test case because it belongs to the group of prototypical SNe Ia and because its spectrum is available over a broad range of wavelengths.

SN 1992A was discovered in NGC 1380 in the Fornax Cluster on 11 Jan. 1992 by Liller (1992), and observed with various instruments. In particular, this was the first SN Ia to be observed with the Hubble Space Telescope (Kirshner et al. 1993). The HST UV spectra, together with simultaneous optical spectra, give a coverage of the SN spectrum from 1630 to 8100Å, which is unprecedented for SNe Ia. The spectral evolution and the light curve of SN 1992A are typical of SNe Ia (the optical spectrum of SN 1992A is almost indistinguishable from that of the prototypical SN Ia, SN 1981B). SN 1992A reached B maximum on 19 Jan. 1992 at $B = 12.6$ mag. The SN light suffered from very little reddening, and E(B-V) was estimated at 0.03 mag. The (B-V) colour at B maximum was 0.0. The HST spectrum of 24 Jan. 1992 corresponds then to an epoch 5 days after B maximum, when SNe Ia are still well within the photospheric epoch.

The importance of testing our model on a spectrum that includes the UV is obvious: since the UV is the spectral region most affected by line blocking, our success in fitting the observations with a synthetic spectrum would show that our model reproduces line blocking correctly.

As mentioned in the previous section, in our model we used the rescaled density structure derived from the 'standard' deflagration model W7. We also used the elemental abundances given by that model, but adopted an abundance mixing at $v > 8000$ km/s, since this is supposed to yield a better reproduction of the observed spectra (Branch et al. 1985).

In the next section we discuss the results of our calculations, and how we refined our models to improve them.

5. Line blocking: the method and results

5.1. Pure continuum model

In our first model we ignored line blocking, i.e. we considered only continuum opacity in the NLTE calculation. In Fig. 2 we show the final run of $\tau_{\rm Ross}$ vs. velocity in the envelope. The $\tau_{\rm Ross}$ calculation extends downwards to < 1000 km/s, i.e. almost to the centre of the SN ejecta. Since the photosphere falls typically at $\tau_{\rm Ross} = 1$, we see that in the model the (time dependent) pseudo-photosphere lies at $v \sim 5000$ km/s. This is rather low when compared to the values typically used for this epoch ($Max + 5$ days, i.e. $t = 25$ days after explosion), which are $v_{ph} \sim 7500$ km/s. This result is easily understood since the contribution of the lines to the opacity is not considered in this pure continuum model. Note that throughout the atmosphere (except for the very deepest layers with $\tau_{\rm Ross} > 10$) Thomson scattering is the exclusive contributor to the (pure continuum) Rosseland optical depth (dashed curve in Fig. 2). Line opacity makes an important contribution to the total opacity in a SN atmosphere at early times, especially in the B and UV regions, where it shifts the pseudo-continuum outwards. In fact, since lines form typically at $\tau_{\rm Ross} \sim 0.1 - 0.3$, it is clear from Fig. 2 that the lines will form at $v > 8000$ km/s. In those spectral regions where line overlap effectively forms a continuum, v_{ph} will indeed be close to that value. Note that in this model the presence of the lines was only considered in the final formal integral calculation.

In Fig. 3, we show the synthetic spectrum obtained for the model without line blocking: not only does the model spectrum not reproduce the flux in the UV, as could be expected, but in the optical the observed line features are not reproduced either. The two strongest features in the synthetic spectrum are due to Fe III lines, which indicates that the ionization is too high because of the excessive UV flux. Actually, these features were dominant in the pre-maximum spectrum of SN 1991T, an overluminous SN Ia where the ionization was consequently higher

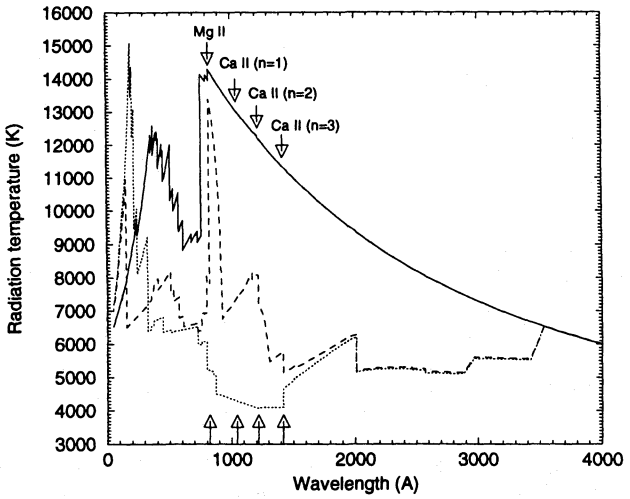

Fig. 4. The emergent radiation temperature (T_R) as a function of wavelength in the three models: pure continuum model (solid line); empirical line blocking case (a) (dotted) and case (b) (dashed).

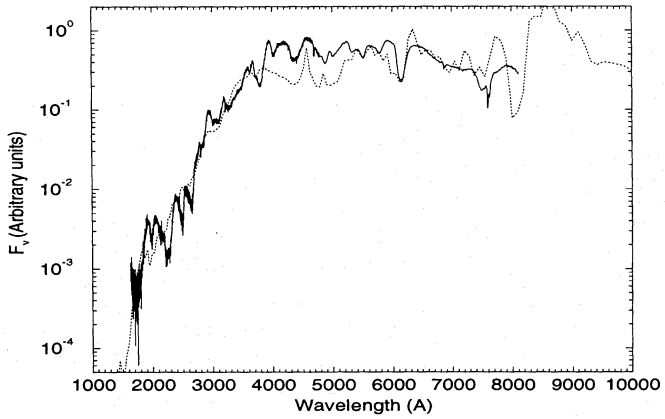

Fig. 5. The synthetic NLTE spectrum for the empirical line blocking case (a) (dotted line) compared to the spectrum of SN 1992A (solid line). Note that the strong absorptions in the region from $\sim$ 4000−5300 Å are mainly due to iron group elements.

than in normal SNe Ia (Mazzali et al. 1995). This confirms the importance of line blocking in the UV and B regions.

5.2. Empirical line blocking

5.2.1. Constraints form the observations

In this method the contribution due to line blocking is considered in the wavelength region where the 'true' continuum is optically thin down to the deepest layers, by *simulating* line opacities and emissivities in such a way that the calculated emergent spectrum is consistent with the observed one (the procedure is described in the Appendix). In this approach, the line opacity is assumed to be a function of frequency and proportional to the density, and the two-level approximation is used for the emissivity. In this way, the opacity term due to strong lines is just an extra additive term to the continuous opacity (see Appendix). Note

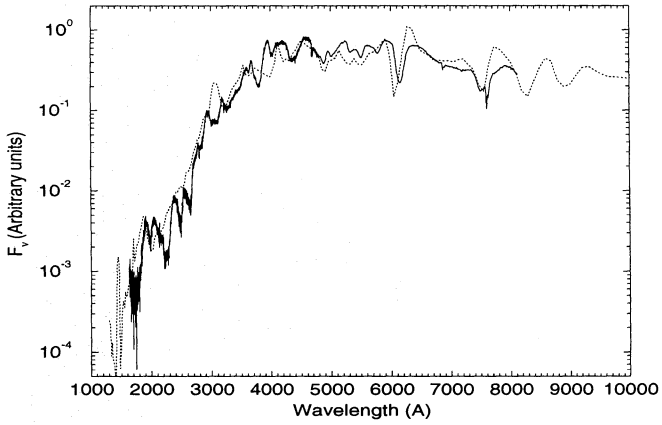

Fig. 6. The synthetic NLTE spectrum for the empirical line blocking case (b) (dotted line) compared to the spectrum of SN 1992A (solid line).

that the diffusion approximation is still used. This backward scheme makes the most of the observations, and is ideal to verify whether line blocking alone can diminish the discrepancy between the synthetic and the observed spectra, especially in the UV. Its validity can be verified by checking whether the temperature, ionization and excitation in the atmosphere which yield a good reproduction of the line-blocked UV flux do the same with the visible part of the spectrum, where line blocking is not so important. The method has the advantage that the amount of line blocking included is guaranteed to be of the correct order, and so it gives also an important constraint for the exact method, which we describe in Sect. 5.3.

When we introduce line blocking from the observed spectrum as described above, we do not know how the spectrum behaves below 1600 Å. So, we performed two numerical experiments, where we simulate the behaviour of the spectrum below 1600 Å. In the first case (a) we assume that the flux drops to zero rapidly below 1600 Å. In case (b), on the other hand, we assume that the flux rises somewhat between 1300 and 800 Å, for reasons that will become clear below.

Below 800 Å, the continuum becomes optically thick in both cases due to bound-free opacities. In Fig. 4 we show the behaviour of the emergent radiation temperatures $T_R(\lambda)$ as the two line blocking approximations are introduced in turn. From Fig. 4 it is clear that line blocking is definitely the most effective source of opacity between 1300 and 3500 Å, and that our two different line blocking appoximations affect mostly the region between 800 and 1300 Å. The two different assumptions for the far-UV flux lead to somewhat different ionization structures and different emergent spectra. In particular, in case (a) the radiation temperatures are modified so that the ionization edges of the Ca II ground state and lowest lying excited states make the continuum optically thick, while in case (b) they do not. Note that the rise of the T_R values for $\lambda < 800$ Å in case (a) is due to the fact that no simulated line opacities are included in the continuum radiation transport calculations below the Mg II ground state edge (824 Å) (see above).

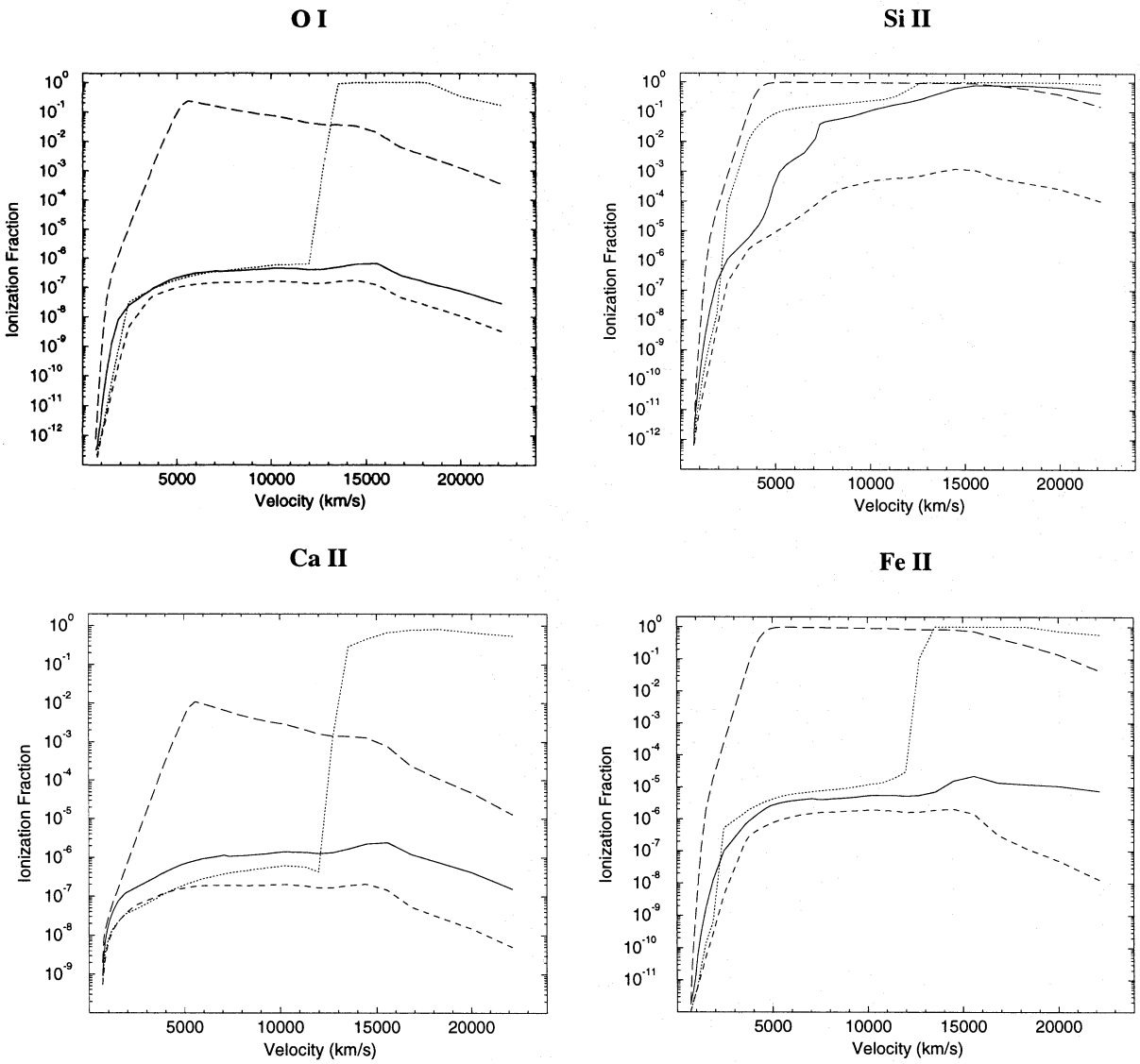

Fig. 7. The ionization fraction vs. velocity in the ejecta for some of the most important ions in a SN Ia spectrum. The curves represent: LTE (long dashed); NLTE continuum opacity only (short dashed); NLTE empirical line blocking case (a) (dotted); NLTE empirical line blocking case (b) (solid line).

The synthetic spectra we obtained are shown in Figs.5 and 6, respectively. The introduction of line blocking allows the observed average flux level to be reasonably well reproduced at all spectral regions in both cases, but the detailed agreement with the spectral features is not very good. In particular, for case (a), lines due to Fe-group elements are not well reproduced in the optical part of the spectrum. If we compare the ionization structure for this model above 10,000 km/s (Fig. 7, dotted lines) with the equivalent SN 1990N model by Mazzali et al. (1993, Figs. 6 and 8), which reproduced the observed optical spectrum well, we see that the fraction of singly ionized (respectively neutral) species of all the main elements (Fe, Co, Ni, Si, S, Ca) is larger in the case (a) model by factors between 10 for Si and 10^4 for Ca and O. The low degree of ionization explains the strength of the Ca II and Si II lines and of the Fe II lines near 5000 Å, and is due to the lack of exciting and ionizing UV photons. Therefore this approximation is too extreme, too much blocking is assumed and the ionization is too low.

As we have shown in Sect. 5.1, neglecting UV line blocking leads to an excessively high UV flux, and to a higher–than–observed degree of ionization, but including too much line blocking, as in case (a) above, gives the opposite result, i.e. not enough flux and lower–than–observed ionization. In case (b), where a smaller empirical line blocking is adopted in the far UV, photoionization from excited levels of species such as Si II, Ca II, Fe II, Co II can take place to some extent due to the stronger radiation field (see Fig. 4). This change has important consequences for the degree of ionization. The net result is that in this model the ionization degree is higher than in case (a), although not as high as in the model where blocking was ig-

nored altogether. In Fig. 6 we show the synthetic spectrum for case (b). The improvement with respect to the case (a) spectrum is clear. Overall the synthetic spectrum resembles the observed one, although problems still remain, such as the weakness of Ca II H&K and of most UV features.

In addition to the case (a) ionization fractions, Fig. 7 also displays the corresponding numbers for the two other models described above as well as the LTE case. Note that in case (a) the rapid transition in the ionization of Ca, O and Fe near 10,000 km/s is due to the presence of the boundary of the Ca III Strömgren sphere: recombination of Ca III into Ca II, which has the redmost ground state ionization edge (1044 Å) among the important ions in the SN Ia composition, leads to an optically thick Ca II continuum (see Fig. 4), and consequently to the recombination of those ions whose ground state ionization edges lie close to that of Ca II, i.e. Fe II (767 Å) and O I (911 Å). In both of these cases, ionization from excited levels is mostly affected by the presence of the optically thick continuum between 800 and 1300 Å. The jump in ionization occurs for Si II (ground state ionization edge at 759 Å) as well, but is less noticeable since this ion is not so depleted in the deeper layers of the atmosphere.

The general effect of line blocking on the ionization structure is clearly visible: the diminished radiation field tends to shift the ionization fractions from the 'high–ionization–regime' of the pure continuum model to the 'low–ionization–regime' of the LTE case. In the outer atmospheric layers case (a) even lies clearly above the LTE case.

In case (b), on the other hand (solid lines in Fig. 7), the ionization is only somewhat lower than in the unblocked model (short dashed lines in Fig. 7) and, with the exception of Si II, distinctly higher than in the LTE case.

One general conclusion is that our empirical blocking model (b) at least reproduces the position of the photosphere, since the average flux level is everywhere well reproduced, but that a more consistent treatment of blocking is required to determine the ionization structure, since we have no observations for the important line-blocking region below 1600 Å.

5.2.2. Constraints from the MC spectrum synthesis model

In order to overcome this problem, we have adopted as a reference flux the result of a model calculation, which was performed by Mazzali et al. (1993; see Sect. 3). We used this MC-model because it has proved able to give good fits to optical spectra from the photospheric epoch of SNe Ia.

In the MC-model, the radiative equilibrium calculation yields the radiation temperature $T_{\rm rad}$ as a function of radius. Neglecting the influence of γ-rays, the electron temperature $T_{\rm e}(r)$ is set to $0.9\,T_{\rm rad}(r)$. These values are used to calculate the ionization and excitation state of the envelope gas, where the level occupation numbers are computed in the nebular approximation (Abbott & Lucy 1985). The effect of line blocking on the ionizing UV continuum is also considered (Mazzali & Lucy 1993), and, together with the emerging spectrum, is computed with a MC method. Line formation is assumed to occur by coherent scattering, and the Sobolev approximation is assumed to hold. Relativistic radiative terms of $O(v/c)$ are included.

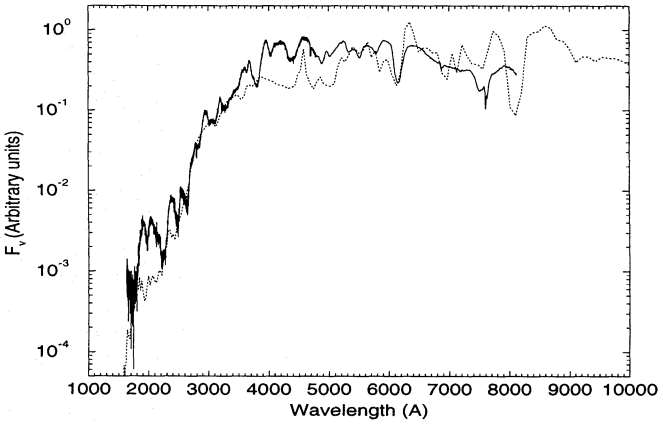

Fig. 8. The synthetic NLTE spectrum for the model using the original MC spectrum as a reference flux and an extended photosphere (dotted line) compared to the spectrum of SN 1992A (solid line).

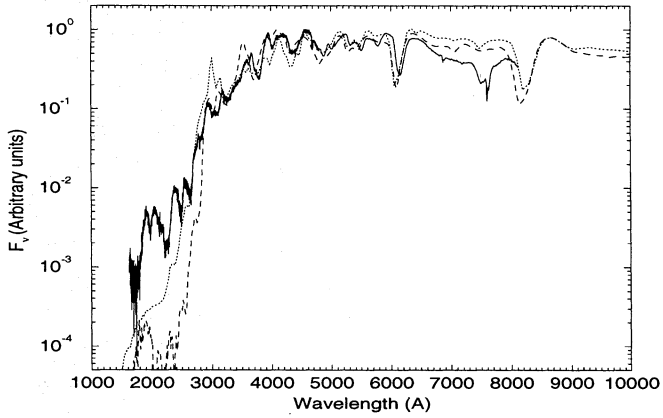

Fig. 9. The synthetic NLTE spectrum for the model using the original MC spectrum as a reference flux and a one-point photosphere (dotted line) compared to the synthetic MC spectrum (dashed line) and to the spectrum of SN 1992A (solid line).

In Fig. 8 we compare the observed spectrum of SN 1992A with our NLTE spectrum, where we have used the above mentioned MC energy distribution as a reference flux for our line blocking calculations. However, our temperature structure was computed as described in Sect. 3. (Note that this was necessary since the MC model assumes a sharp photosphere (falling at $\tau_{\rm Ross} \sim 2/3$), and does not give $T_{\rm e}$ values at lower velocities, but these are needed for the NLTE calculation with an extended photosphere. The one-point photosphere assumption in the Monte Carlo model also leads to an increased temperature gradient above the photosphere, since the rise to high temperatures in deep layers has to be realized at and above the photosphere in this model.)

The low UV flux below 2700 Å clearly shows that the NLTE spectrum overestimates line blocking. This in turn affects the ionization structure, so that several optical features are not well reproduced. Overall, the ionization appears too low (lines of

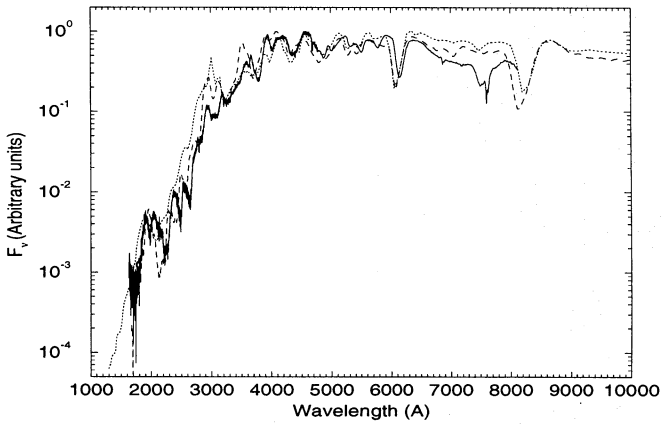

Fig. 10. The synthetic NLTE spectrum for the model using the improved MC spectrum as a reference flux and a one-point photosphere (dotted line) compared to the synthetic MC spectrum (dashed line) and to the spectrum of SN 1992A (solid line).

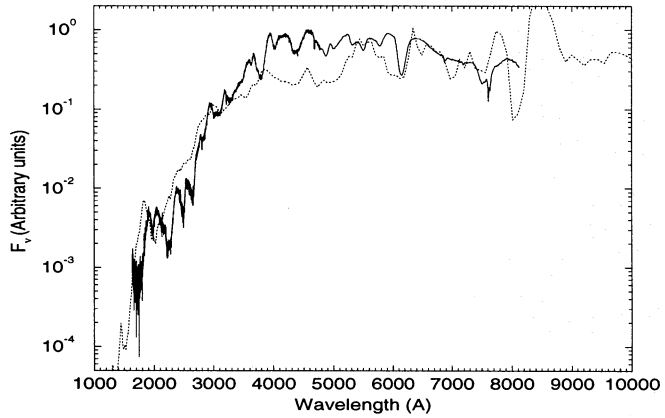

Fig. 11. The synthetic NLTE spectrum for the model using the improved MC spectrum as a reference flux and an extended photosphere (dotted line) compared to the spectrum of SN 1992A (solid line).

Ca II and Fe II are strong, while S II is weak), and the synthetic spectrum resembles that of case (*a*) above (cf. Fig. 5).

In order to investigate the reason for these discrepancies, next we calculated a NLTE model with a one-point photosphere – as in the MC model –, hence also keeping the temperature structure of the MC model. The resulting spectrum is shown in Fig. 9(dotted line). The results are very similar to the MC (dashed line) as well as to the observed spectrum in the optical part. In the near-UV the flux level is still reasonable, but the detailed agreement of the observed features is poor. At $\lambda < 2500$ Å, on the other hand, where Fe II and Co II lines dominate, neither the continuum level nor the lines are well reproduced by the model. This shows that the blocking calculated with the MC model is too strong (note that the flux depression is even more pronounced in the MC model).

This is the case because the excitation and ionization in the MC model are based on the assumption of an optically thin ionization continuum (i.e. the depression due to continuum opacity is neglected). Using the experience acquired from the empirical

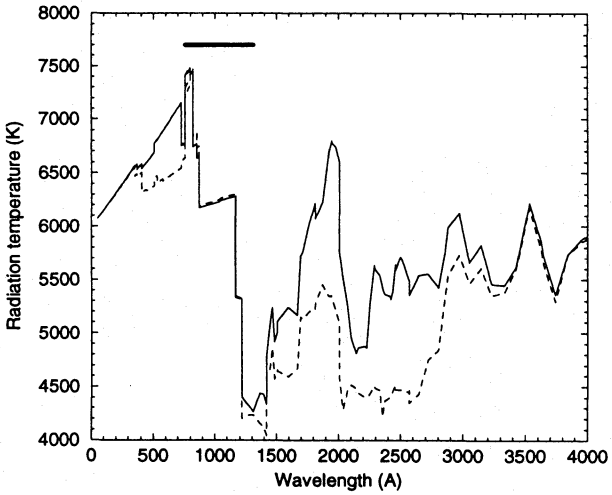

Fig. 12. The emergent radiation temperature (T_R) as a function of wavelength in the NLTE models with the energy distribution of the MC models as a reference flux and an extended photosphere: dashed line: original MC model; solid line: improved MC model.

blocking calculations in Sect. 5.2.1, which clearly showed that the ionization continuum becomes optically thick at $\lambda \lesssim 1500$ Å due to line blocking, and is greatly reduced below about 3000 Å, and applying the modified ionization equation given by Mazzali & Lucy(1993) in their Eq. 18, we computed a new MC model, where we assumed that the transition from the optically thin to the optically thick continuum occurs at 2800 Å.

When this new approximation is introduced, the synthetic MC spectrum improves greatly in the UV, as shown in Fig. 10 (dashed line). The optical part, on the other hand, is not very much affected. The NLTE synthetic spectrum obtained using this improved MC spectrum and a one-point photosphere with the MC temperature structure (dotted line in Fig. 10) is substantially better in the UV than the spectrum obtained with the original MC spectrum (cf Fig. 9). It resembles the MC spectrum closely, but in the UV the flux is somewhat too high and the lines are not sufficiently strong, while in the optical the agreement is of the same quality.

However, even the improved MC model probably overestimates line blocking, as shown by the fact that the MC synthetic spectrum is completely blocked below 1500 Å. This is more clearly illustrated by Fig. 12, where the run of the emergent radiation temperatures $T_R(\lambda)$ vs. λ as obtained from the NLTE models with extended photospheres based on the original (dashed line) and the improved (solid line) MC spectrum are shown. (Note that due to the resulting zero fluxes in the region between $\sim$ 800 and 1300 Å in both MC models (horizontal bar in Fig. 12), no information can be inferred concerning the correct value of flux reduction in this important wavelength range.)

The NLTE spectrum obtained using the improved MC fluxes with an extended photosphere, shown in Fig. 11, still suffers from problems in the ionization structure, similar to the empirical blocking model (*a*) (Fig. 5) and to the model computed with the original Monte Carlo fluxes and an extended photo-

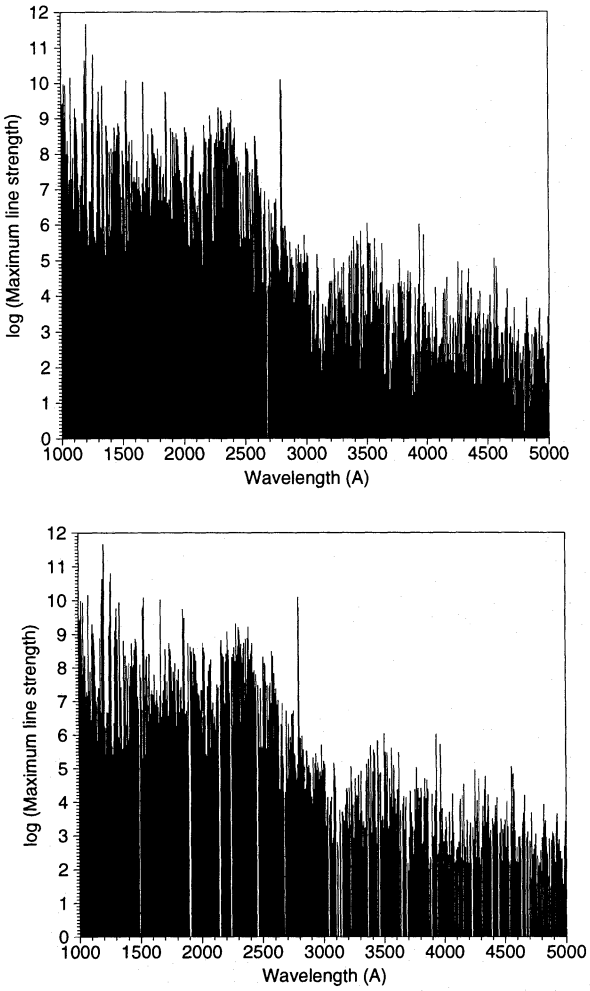

Fig. 13. Wavelength dependent distribution of the lines before (upper panel) and after (lower panel) the line reduction. The plotted quantity 'line strength' is defined as the ratio of the frequency integrated line opacity to the Thomson opacity.

sphere (Fig. 8). This indicates that the NLTE model with the extended photosphere yields a lower degree of ionization compared to the NLTE model with the one-point photosphere. The reason for this behaviour has to be attributed to the inconsistent treatment of the photospheric region: the photosphere is correctly calculated in the former NLTE case, but is reduced to the simplest case for the computation of the emergent radiation temperatures obtained from the MC model.

5.3. Consistent blocking

Given the various problems mentioned in the previous sections, it was clear that a model where line blocking is included explicitly had to be computed. The first step in this direction is to perform a line reduction which allows a reasonable number of lines (typically the 200 strongest per overlap interval $\Delta\nu/\nu = 2v_{\max}/c$) to be treated without loss of significance in the total opacity calculation. Fig. 13 shows the distribution in frequency of the lines before and after the line reduction.

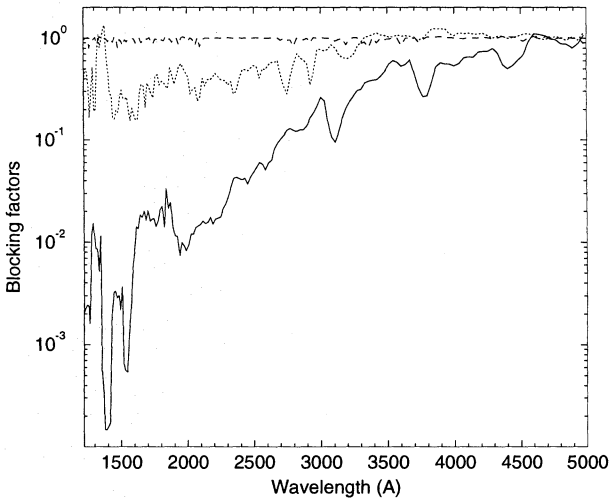

Fig. 14. Converged solution of the blocking factors (J^{C+L}/J^{C}) as a function of wavelength at 3 depths in the ejecta: near the effective photosphere (6,500 km/s, dotted curve), very deep in the ejecta (2,000 km/s, dashed curve) and very far out (20,000 km/s, solid curve).

Secondly, instead of computing mean opacities and emissivities over the various frequency intervals, we calculated mean intensities $(J_\nu^{C+L})_f$ in the formal integral (accounting for all contributing opacities, i.e. continuum *and* lines), since this approach avoids the disadvantages of opacity averaging. These values are then used in the NLTE code iteratively. This procedure is incorporated in our ALI.

The implementation of the $(J_\nu^{C+L})_f$ values with line blocking is performed using 'blocking factors'. In practice, the mean intensities obtained as described above are divided by the $(J_\nu^{C})^{old}$ values from the previous iteration of the NLTE code including only the continuum opacity. We then adopt a 'modified' radiation field computed as:

$$J_\nu^{mod} = (J_\nu^{C})^{new} \frac{(J_\nu^{C+L})_f}{(J_\nu^{C})^{old}}, \tag{1}$$

where $(J_\nu^{C})^{new}$ is the radiation field obtained in the present ALI cycle with the actual NLTE continuum opacities (of course now without any additional simulated contributions). Using this modified radiation field, new radiative rates R_{ij} (both continuum and lines) are calculated, and the resulting NLTE occupation numbers are used in the next solution of the formal integral. This procedure is iterated until convergence (see below).

Clearly, at practically all wavelengths (and except for the innermost atmospheric layers), $J^{C+L} \leq J^{C}$. Fig. 14 shows the converged solution of the ratio J^{C+L}/J^{C}, ('blocking factors') in the UV and optical at 3 different velocities in the ejecta: near the effective photosphere (6,500 km/s, dotted curve), very deep in the ejecta (2,000 km/s, dashed curve) and very far out (20,000 km/s, continuous curve). At very low velocities the UV continuum is optically thick, due mostly to excited level ionization edges, and the lines have a negligible influence, so $J^{C+L} \simeq J^{C}$. Near the photosphere the effect of blocking is clearly seen: at $\lambda \sim 2000$ Å, $J^{C+L}/J^{C} \sim 0.2$. This means that the lines have a

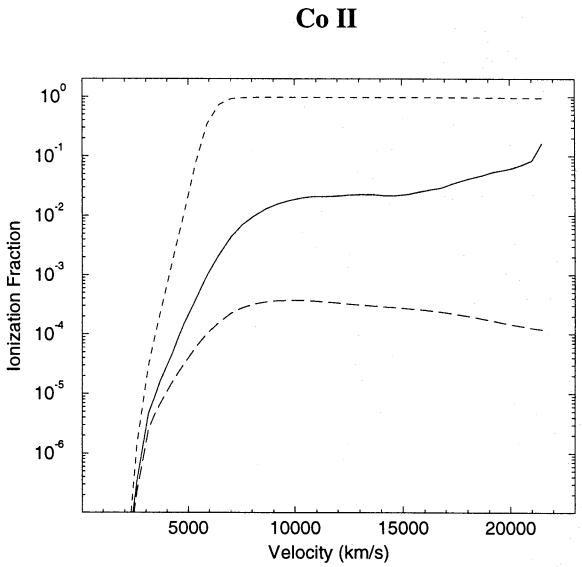

Fig. 15. The Co II ionization fraction vs. velocity in the ejecta as a test of the convergence of the iteration: the two dashed curves represent the initial ionization structure, depending on the adopted starting approximation: full blocking (long dashed); no blocking (short dashed). The solid curve is the result in both cases.

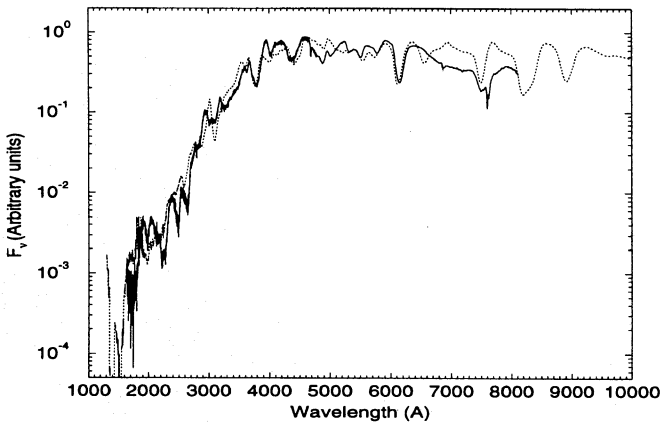

Fig. 16. The synthetic NLTE spectrum for the consistent blocking model (dotted line) compared to the spectrum of SN 1992A (solid line).

dominating effect. Going towards optical wavelengths, though, line blocking decreases, and again $J^{C+L} \simeq J^{C}$. The contribution to the continuum opacity is from excited level ionization edges, as already shown in Fig. 4. Finally, very far out in the ejecta, the continuum opacity is negligible due to the low density, and the J^{C+L}/J^{C} ratio reflects just the density of strong lines (cf. Fig. 13), so it lies below the per cent level in the UV, where line blocking is very efficient, and has a value ~ 0.5 in the blue, since the lines do not totally absorb the radiation field.

The reader may note that in the iteration scheme convergence is achieved regardless of the starting approximation, as shown in Fig. 15, where we plot the result for the Co II ionization fraction: the two dashed lines correspond to two different initial blocking assumptions: fully blocked (short dashed), i.e. low ionization; unblocked (long dashed), i.e. high ionization. The continuous line, which is actually the superposition of two almost identical curves, is the result in both cases. The resulting spectrum is shown in Fig. 16. The agreement with the observations is indeed quite good, especially considering that this is only a first result, where parameters have not been tuned. Both the flux level and most line features are now reasonably well reproduced throughout the spectrum.

Finally, in Fig. 17 we show the behaviour of the ionization of the same elements as above. Compared with the results of the empirical blocking models (Fig. 7), we find that the tendency to lower the degree of ionization is even more pronounced in the model with consistent blocking. This affects in particular ions like Fe II, O I, Ca II. On the other hand, comparing these plots with Figs. 6 and 7 in Mazzali et al. (1993) shows that the ionization results are very similar for the region above the photosphere.

6. Conclusions

We have presented our method to calculate synthetic early-time spectra of SNe Ia. Besides a detailed NLTE treatment, we have considered explicitly the effect of line blocking. Our models have been computed using the best available atomic data and all important contributions to the rate equations, and a very fine frequency grid for the solution of the transfer equation to yield the emergent spectrum.

We have shown that the SN Ia atmosphere is electron scattering-dominated, and that line blocking is a very important contributor to the opacity, especially in the UV. Moreover, it turned out in our calculations that a correct treatment of the photosphere is fundamental for a realistic computation of the ionization structure and that the apparent high–velocity–photosphere in the SN at early times is due to the line–blocking–induced opacity, since the continuous optical depth only reaches values close to unity at large depths in the ejecta ($v \sim 5000$ km/s), even at an early epoch. We also found that the effect of NLTE on the ionization structure obtained from calculations neglecting line opacities are quite drastic (up to six dex in the ionization fractions of low ionization stages, e.g. O I), whereas the effect of line blocking is to extend the effectively optically thick part of the spectrum to wavelengths up to $\lambda \sim 1300$Å, thus reducing the ionization from the excited levels of several important ions (e.g. Fe II, Co II, Si II, Ca II, O I) and hence reducing the NLTE effect. This has the misleading consequence that LTE seems to be not too bad an approximation.

We have shown that various empirical treatments of line blocking can yield a reasonable synthetic spectrum, but that they depend heavily on the approximation used for the flux in the unobserved far-UV, between 800 and 1300Å. Inaccuracies in the treatment of line blocking can lead to very different results with respect to the ionization structure and the emergent spectrum.

Emergent radiation temperatures from models based on the synthetic spectra computed with a MC code, which assumes a one-point photosphere, also have shortcomings. The transfer of these data to the extended photosphere case is not successful,

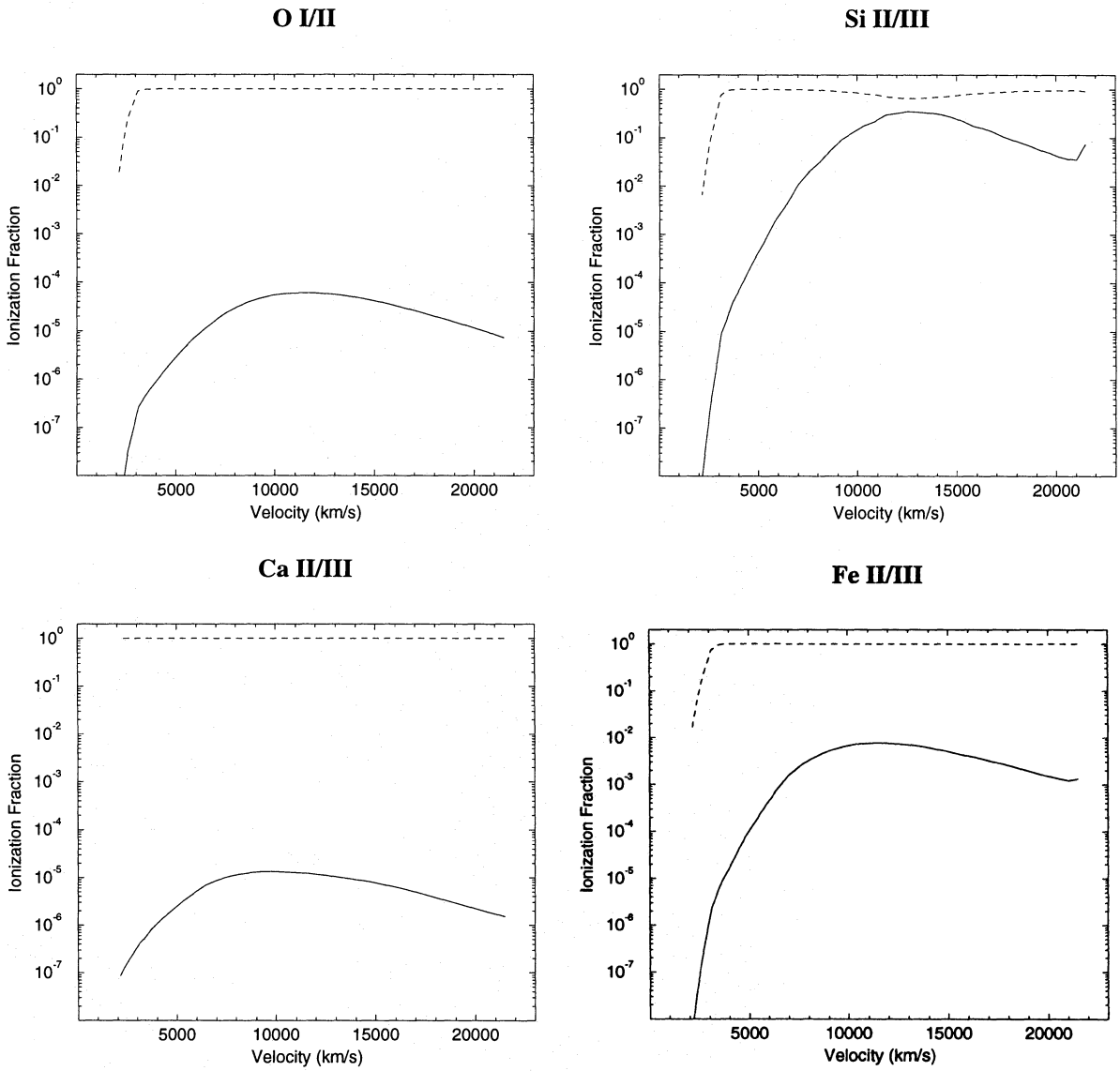

Fig. 17. The ionization fraction resulting from the consistent blocking model vs. velocity in the ejecta for some of the most important ions in a SN Ia spectrum. For each element, the solid line represents the lower of the two ionization stages shown, as marked in the header.

because line blocking in the far-UV at low ejecta velocities (below the position of the MC photosphere and below 1500 Å) is overestimated and the $\tau_{\rm Ross}$ = 1-point is therefore reached too far out in the ejecta.

Only a model where line blocking is dealt with in a consistent form predicts a reasonable ionization structure. In this case the emergent NLTE spectrum reproduces the spectrum of the 'standard' SN Ia 1992A quite well from the UV to the near-IR.

However, there is still some way to go in order to obtain 'realistic' spectra of SNe Ia:

- The proposed chemistry and density structure of realistic explosion models should be applied.
- The ionizing effect of the fast electrons produced by the γ-rays from the decay of ^{56}Ni and ^{56}Co should be treated properly.

In the next step our method will be improved in order to overcome these shortcomings.

Acknowledgements. It is a pleasure to thank Prof. Dr. R.P. Kudritzki, Prof. Dr. D. Branch, Dr. L. Lucy, Dr. A. Fullerton, Dr. K. Butler, G. Taresch, Dr. E. Müller and Dr. P. Höflich as well as our referee, Prof. Dr. F.-K. Thielemann, for discussions and comments, and B. Springsteen and F. Gump for emotional support. This work was supported by the Deutsche Forschungsgemeinschaft under grant Pa 477/1-1. P.A.M. acknowledges the Italian Ministry of University and Research (M.U.R.S.T.) and the Italian National Research Council (C.N.R.) for travel support.

Appendix A: the empirical line blocking method

Here we present the principles of our approximate treatment of line blocking, which is based on the simulation of the line opacities and

emissivities as constrained by the observed or synthetic MC spectrum (see Sect. 5.2). Starting from the assumption that the line opacities are linearly proportional to the electron density (n_e):

$$\chi_\nu^{bb} = a_\nu n_e, \tag{A1}$$

spatially constant factors a_ν are defined which are a function of frequency only. Using the two-level approximation, the source function is given by:

$$S_\ell = \epsilon B_\nu + (1-\epsilon) J_\nu, \tag{A2}$$

with

$$\epsilon = \frac{\epsilon'}{1+\epsilon'} \tag{A3}$$

and

$$\epsilon' = (1 - e^{\frac{h\nu}{kT}}) \frac{C_{ul}}{A_{ul}}, \tag{A4}$$

where the ratio of the collisional deexcitation rate (C_{ul}) and the Einstein spontaneous emission probability (A_{ul}) can be expressed in terms of the Van Regemorter (1962) formula:

$$\frac{C_{ul}}{A_{ul}} = \frac{n_e}{T^{1/2}} \frac{10.339}{\nu/c^3}. \tag{A5}$$

Thus, for given factors a_ν the line opacities and emissivities

$$\eta_\nu^{bb} = \chi_\nu^{bb} S_\ell \tag{A6}$$

can be treated as additional terms in a second step of the continuum radiative transfer.

However, for all frequency intervals where line blocking dominates, mean values of the factors a_ν have to be calculated in advance by means of an approximate solution of the radiative transfer equation, where the diffusion approximation is required at the lower boundary and the observed values of the UV flux have to be taken as an outer boundary condition so that they can be reproduced as the output of the correct continuum radiative transfer after the introduction of the blocking factors.

For the approximate solution we consider the second moment of the radiative transfer equation:

$$\frac{\partial K_\nu}{\partial r} + \frac{1}{r}(3K_\nu - J_\nu) = -\kappa_\nu H_\nu, \tag{A7}$$

and use for the first three moments (J_ν, H_ν, K_ν) of the specific intensity (I_ν) the simplifying quadratures proposed by Lucy (1971), which give:

$$K_\nu = \frac{1}{3}(J_\nu + 2\mu_* H_\nu) \tag{A8}$$

with

$$\mu_* = (1 - (R/r)^2)^{1/2}, \tag{A9}$$

where R is the innermost radius in the model.

Elimination of K_ν and substitution of the derivative of H_ν with the first moment of the transfer equation then gives:

$$\frac{\partial J_\nu}{\partial r} = \frac{2R\mu_*}{x^2}(\eta_\nu - \kappa_\nu J_\nu) + H_\nu\left(\frac{2}{x\mu_*} + 3\kappa_\nu \frac{R}{x^2}\right) \tag{A10}$$

with $x = R/r$.

In the blocking dominated part of the atmosphere the right hand side of the above equation can be approximated by the last term, and apart from Thomson scattering, continuous absorption can be neglected. Integrating and using Eq. A1 we obtain:

$$\begin{aligned}\Delta J_\nu &\simeq B_\nu(T(x_{\tau_f})) - W_{x_0} B_\nu(T_{\rm rad}) \simeq B_\nu(T(x_{\tau_f})) \\ &= 3R(\bar{a}_\nu + \sigma_e)\int_{x_0}^{x_{\tau_f}} \frac{H_\nu}{x^2} n_e dx\end{aligned} \tag{A11}$$

where $W(x) = \frac{1}{2}(1-\mu_*)$ is the geometrical dilution factor, $T_{\rm rad}$ is the radiation temperature of the emergent (observed) flux in the considered interval, σ_e is the Thomson cross section, x_0 is the outermost point and τ_f is the optical depth which separates the regime where the diffusion approximation can be applied from that where we assume an optically thin continuum. Due to the latter assumption, H_ν can be approximated by

$$H_\nu(x) = x^2 \left(\frac{R_p}{R}\right)^2 \frac{1}{4} B_\nu(T_{\rm rad}) \tag{A12}$$

where R_p refers to the photospheric radius. Eq. A12 allows us to rewrite Eq. A11 for $\bar{a}_\nu/\sigma_e$ as

$$\frac{\bar{a}_\nu}{\sigma_e} \simeq \frac{B_\nu(T(x_{\tau_f}))}{B_\nu(T_{\rm rad})} \left(\frac{3}{4}\frac{R_p^2}{R}\int_{x_0}^{x_{\tau f}} \sigma_e n_e dx\right)^{-1} - 1 \tag{A13}$$

After evaluating Eq. A13 according to τ_f, the continuum radiative transfer can be solved correctly. In order to reproduce the pre-specified emergent fluxes ($T_{\rm rad}$) in the line–blocking–dominated part sufficiently well – i.e. within a few percent – the uniform value τ_f is adjusted iteratively. Depending on the model, values between 3 and 8 are obtained for τ_f.

References

Abbott D.C., Lucy L.B., 1985, ApJ 288, 679

Branch D., Doggett J.B., Nomoto K., Thielemann F.-K., 1985, ApJ 294, 619

Branch D., Pauldrach A.W.A., Puls J., Jeffery D.J., Kudritzki R.P., 1991, in: ESO/EIPC Workshop Supernova 1987A and other Supernovae, Danziger I.J., Kjär K.(eds.). ESO, Garching, p.437 (ELBA)

Duschinger M., Puls J., Branch D., Höflich P., Gabler A., 1995, A&A 297, 802

Eissner W., Jones M., Nussbaumer H., 1974, Comput. Phys. Commun. 8, 270

Filippenko A.V., Richmond M.W., Branch D., et al., 1992, AJ 104, 1543

Harkness R.P., 1991, in: Supernovae: The Tenth Santa Cruz Workshop in Astronomy and Astrophysics, Woosley S.E.(ed.). Springer-Verlag, New York, p.454

Höflich P., 1995, ApJ 443, 89

Jeffery D.J., Leibundgut B., Kirshner R.P., et al., 1992, ApJ 397, 304

Kirshner R.P., Jeffery D.J., Leibundgut B., et al., 1993, ApJ 415, 589

Kurucz R.L., 1992, Rev. Mex. Astron. Astrofis. 23, 181

Liller W., 1992, IAU Circ., No. 5428

Lucy L.B., 1971, ApJ 163, 95

Mazzali P.A., Lucy L.B., 1993, A&A 279, 447

Mazzali P.A., Lucy L.B., Danziger I.J., et al., 1993, A&A 269, 423

Mazzali P.A., Danziger I.J., Turatto M., 1995, A&A 297, 509

Nomoto K., Thielemann F.-K., Yokoi K., 1984, ApJ 286, 644
Nugent P., Baron E., Hauschildt P.H., Branch D., 1995, ApJ 441, L33
Pauldrach A., 1987, A&A 183, 295 (Paper III)
Pauldrach A., Herrero A., 1988, A&A 199, 262
Pauldrach A.W.A., Kudritzki R.P., Puls J., Butler K., Hunsinger J., 1994, A&A 283, 525 (Paper XII)
Puls J., Hummer D.G., 1988, A&A 191, 87
Van Regemorter H., 1962, ApJ 136, 906

This article was processed by the author using Springer-Verlag LaTeX A&A style file *L-AA* version 3.